

Numerical Computation of Pressure in a Rigid Rectangular Tank due to Large Amplitude Liquid Sloshing

Hakan AKYILDIZ, M. Serdar ÇELEBİ

*Istanbul Technical University, Faculty of Naval Architecture and Ocean Engineering,
80626, Maslak, İstanbul-TURKEY*

Received 11.02.2000

Abstract

In this study, sloshing inside partially filled enclosed baffled and unbaffled tanks was investigated. The fluid is assumed to be homogeneous, isotropic, viscous, and Newtonian and exhibiting only limited compressibility. Tank and fluid motions are assumed to be two-dimensional. A moving coordinate system is employed so that the tank movement is set to rest. The volume of fluid technique will, then, be used to track the free surface. The model solves the complete Navier-Stokes equations in primitive variables by the use of finite difference approximations. At each time step, a donor-acceptor method is used to transport the volume of fluid function and hence the locations of the free surface. Ten different cases including baffled and unbaffled tanks with different fill depths are studied near and on the resonant frequency. In order to assess the accuracy of the method used, computations are compared with theoretical and experimental results.

Key Words: Sloshing, Free surface flow, Navier-Stokes equations, Volume of fluid technique, Finite difference method

Rijit bir Dikdörtgen Tanktaki Büyük Genlikli Sıvı Çalkantısının Oluşturduğu Basıncın Sayısal Hesaplanması

Özet

Bu çalışmada kısmi dolu, kapalı, levhali ve levhasız tankların içindeki sıvı çalkantı hareketleri incelenmiştir. Tank içindeki akışkan homojen, isotropik, viskoz ve belirli oranda sıkıştırılabilir kabul edilmiştir. Tank ve buna bağlı olarak akışkan hareketleri iki boyutlu ele alınmıştır. Hesaplamalarda hareketli koordinat sistemi kullanılmıştır. Bunun sonucunda Navier-Stokes denklemlerinde ek bir ivme terimi ve tank yüzeylerinde ise homojen sınır koşulları oluşmuştur. Ayrıca serbest yüzeyi tanımlamada akışkan hacmi tekniği uygulanmıştır. Kurulan model sonlu farklar yöntemini kullanarak ilkel değişkenlerde Navier Stokes denklemlerini çözmektedir. Her zaman adımında akışkan hacim fonksiyonunun yer değiştirmesini ve buna bağlı olarak serbest yüzey konumunu tespit etmek için “donor-acceptor” yöntemi uygulanmaktadır. Farklı su derinliklerinde sönümleyicili veya sönümleyicisiz on farklı tank kombinasyonu için rezonans frekansında ve civarında hesaplamalar yapıp sunulmuştur. Kullanılan metodun geçerliliğini göstermek amacıyla hesaplamalar deneysel ve teorik sonuçlarla mukayese edilmiştir.

Anahtar Sözcükler: Çalkantı, Serbest yüzey akışı, Navier-Stokes denklemleri, Akışkan hacmi tekniği, Sonlu farklar metodu

Introduction

Liquid sloshing in a moving container constitutes a broad class of problems of great practical importance with regard to the safety of transportation systems, such as tank trucks on highways, liquid tank cars on railroads, and the sloshing of liquid cargo in ocean-going vessels. It is known that partially filled tanks are prone to violent sloshing under certain motions. The large liquid movement will create highly localized impact pressure on tank walls which may in turn cause structural damage and may even create sufficient moment to effect the stability of the vehicle which carries the container. When a tank is partially filled with fluid, a free surface is present. The rigid body acceleration of the tank produces a subsequent sloshing of the fluid. Two major problems arise in a computational approach to sloshing:

- i) The moving boundary conditions at the fluid tank interface,
- ii) The nonlinear motion of the free surface.

Therefore, in order to include nonlinearity and avoid the complex boundary conditions of moving walls, a moving coordinate system is used. The origin of the coordinate, which coincides with the undisturbed free surface, rotates about a fixed axis in Newtonian space.

There are cases where solutions to the nonlinear problem cannot be obtained analytically. Examples are studies of baffled tanks or tanks with complicated geometry. It is then desirable to obtain a numerical solution for the sloshing problem. Early computational fluid dynamic studies effectively used the stream function vorticity approach for the simulation of incompressible fluid dynamics. In this approach, there exists the difficulty of formulating the boundary conditions at the free surface (Roache, 1972). In the present problem with the free surface, the first method using the pressure and velocity as the primary dependent variables was the Marker and Cell (MAC) method developed in the early 1960s (Harlow and Welch, 1965). The MAC method employs an explicit Eulerian finite difference scheme to solve the time dependent Navier-Stokes equations for a viscous incompressible fluid.

Over the years, many improvements have been made to the MAC method, which is based on the refined MAC method. This method can be used for the numerical simulation of sloshing when the free surface motion remains gentle. However, sloshing is not

a gentle phenomenon even at very small amplitude excitations. The fluid motion can become highly non linear, surface slopes can approach infinity and the fluid may encounter the tank top in enclosed tanks. Hirt and Nichols (1981) developed a method known as the volume of fluid (VOF). This method allows steep and highly contorted free surfaces. The flexibility of this method suggests that it could be applied to the numerical simulation of sloshing and is therefore used as the basis in this study.

The analytic study of the liquid motion in an accelerating container is not new. Abramson (1966) provides a rather comprehensive review and discussion of the analytic and experimental studies of liquid sloshing that took place prior to 1966. The advent of high speed computers, the subsequent maturation of computational techniques for fluid dynamic problems and other limitations mentioned above have allowed a new and powerful approach to sloshing, the numerical approach. Von Kerczek (1975), in a survey paper, discusses some very early numerical models of a type of sloshing problem, the Rayleigh-Taylor instability. Feng (1973) used a three-dimensional version of the marker and cell method to study sloshing in a rectangular tank. This method consumes large amount of computer memory and CPU time and the results reported indicate the presence of instability. Faltinsen (1974) suggests a nonlinear analytic method for simulating sloshing, which satisfies the nonlinear boundary condition at the free surface.

Nakayama and Washizu (1980) used a method that basically allows large amplitude excitation in a moving reference frame. The nonlinear free surface boundary conditions are addressed using an "incremental procedure". This appears to be the first study to employ a moving reference frame for the numerical simulation of sloshing.

Sloshing is characterized by strong nonlinear fluid motion. If the interior of a tank is smooth, fluid viscosity plays a minor role. This makes possible the potential flow solution for sloshing in a rigid tank. One approach is to solve the problem in the time domain with complete nonlinear free surface conditions (Faltinsen 1978). Dillingham (1981) addressed the problem of trapped fluid on the deck of fishing vessels, which sloshes back and forth and could result in destabilization of the fishing vessel. Lui and Lou (1990) studied the dynamic coupling of a liquid-tank system under transient excitation analytically for a two-dimensional rectangular rigid tank with no baffles. They showed that the discrepancy in responses

of two systems can obviously be observed when the ratio of the natural frequency of the fluid and the natural frequency of the tank are close to unity. So-laas and Faltinsen (1997) applied Moiseev's procedure to derive a combined numerical and analytical method for sloshing in a general two-dimensional tank with vertical sides at the mean waterline. A low-order panel method based on Green's second identity is used as part of the solution. Celebi et al. (1998) applied a desingularized boundary integral equation method (DBIEM) to model the wave formation in a three-dimensional numerical wave tank using the potential theory. A recent paper by Lee and Choi (1999) studied the sloshing in cargo tanks including the hydro elastic effects. They described the fluid motion by a higher-order boundary element method and the structural response by a thin plate theory.

If the fluid is assumed to be homogeneous and the flow remains laminar, approximating the governing partial differential equations through difference equations would lead to the solution of the sloshing problem. The governing equations are Navier-Stokes equations, and they represent a mixed hyperbolic-elliptic set of nonlinear partial differential equations for an incompressible fluid. The location and transport of the free surface in the tank was addressed using a numerical technique known as the volume of fluid technique. The volume of fluid method is a powerful method based on a function whose value is unity at any point occupied by fluid and zero elsewhere. In this technique, the flow field was discretized into many small control volumes. The equations of motion were then satisfied in each control volume. At each time step, a donor-acceptor method is used to transport the fluid through the mesh. It is an extremely simple method, requiring only one pass through the mesh and some simple tests to determine the orientation of the fluid.

Mathematical Formulation

The fluid considered is assumed to be homogeneous, isotropic, viscous and Newtonian, exhibiting only limited compressibility. Tank and fluid motions are assumed to be two-dimensional, which implies that there is no variation of fluid properties or flow parameters in directions orthogonal to the plane of motion. The domain considered here is a rigid rectangular container with (or without) a baffle partially filled with liquid.

Boundary conditions

Before attempting to solve the governing equations, namely the Navier-Stokes equations, it is necessary to impose appropriate physical conditions on the boundaries of the fluid domain. On the solid boundary, the fluid velocity equals the velocity of the body. In a viscous fluid, the existence of a shear stress requires that both the normal and tangential components of fluid velocity must vanish

$$\vec{V}_n = 0 \quad , \quad \vec{V}_t = 0 \quad (1)$$

where \vec{V}_n and \vec{V}_t are normal and tangential components of the fluid velocity respectively.

The location of the free surface cannot be predetermined, which presents a problem when boundary conditions are to be applied. If free surface boundary conditions are not applied at the proper location, the momentum may not be conserved and this would yield incorrect results. Tangential stresses are negligible because of the larger fluid density compared to the air. The other reason is to avoid satisfying the third free surface boundary condition simultaneously with the kinematic and dynamic free surface boundary conditions. Thus, the only stress at such a surface is the pressure. Therefore, the summation of the forces normal to the free surface must be balanced by the atmospheric pressure. This yields the dynamic boundary condition at a free surface

$$p = p_{ATM} + 2\nu \left\{ n_x t_x \frac{\partial(\rho u)}{\partial x} + n_x t_y \left[\frac{\partial(\rho u)}{\partial y} + \frac{\partial(\rho v)}{\partial x} \right] + n_y t_y \frac{\partial(\rho v)}{\partial x} \right\} = 0 \quad (2)$$

where p_{ATM} , ν and ρ are the atmospheric pressure, kinematic viscosity and density of the fluid, respectively and n and t are the normal and tangential components of unit vector, n_x , t_x are the corresponding horizontal values of the components of the unit vector; n_y , t_y are the corresponding vertical values of the components of the unit vector, on the Cartesian coordinates respectively.

In addition, it is necessary to impose the kinematic boundary condition that the normal velocity of the fluid and free surface are equal.

Conservation of mass and momentum

The conservation laws of physics can be related to a group of fluid particles so that we always exam-

ine the same group of particles. Thus, we define the equation that,

$$\frac{D\rho}{Dt} + \nabla \cdot \rho \vec{V} = 0. \quad (3)$$

For an incompressible fluid, ρ would be constant and the fluid would be non-divergent. In this study, unsteady motion takes place. The characteristic time during the flow changes may be very small. Therefore, the compressibility of fluid may not be ignored. In some cases, it is desirable to assume that the pressure is a function of density.

$$\frac{dp}{d\rho} = c^2 \quad (4)$$

where c is the adiabatic speed of sound. Expanding the conservation of mass equation about the constant mean density ρ_0 and retaining only the lowest order terms yields

$$\frac{1}{c^2} \frac{\partial p}{\partial t} + \rho_0 \nabla \cdot \vec{V} = 0. \quad (5)$$

The forces acting on the fluid in order to conserve momentum must balance the rate of fluid momentum change per unit volume. This principle is expressed as

$$\frac{\partial}{\partial t} (\rho \vec{V}) + \vec{V} \cdot \nabla (\rho \vec{V}) = -\nabla p + \vec{F} + \nu \nabla^2 (\rho \vec{V}), \quad (6)$$

where p is the pressure and \vec{F} is the body force(s) acting on the fluid.

The coordinate system and body forces

In order to include nonlinearity and avoid the complex boundary conditions of moving walls, one uses a moving coordinate system. The origin of the coordinate, which coincides with the undisturbed free surface, rotates about a fixed axis in Newtonian space (see Figure 1).

The equilibrium position of the tank relative to the axis of rotation is defined by ϕ . The tank, at $\phi = 90^\circ$, is rotating about a fixed point on the y -axis. Thus the moving coordinate system can be used to represent the general roll (displayed by θ) and pitch of the vessel.

We suppose that the moving frame of reference is instantaneously rotating with an angular velocity $\vec{\Omega}(\dot{\theta})$ about a point O which itself is moving rel-

ative to the Newtonian frame with acceleration \vec{U} . The absolute acceleration of an element is then

$$\vec{A} = \vec{U} + \vec{a}^* \quad (7)$$

where \vec{a}^* is the acceleration of an element relative to the point O. Here, \vec{a}^* is represented by

$$\vec{a}^* = \frac{\partial^2 \vec{r}}{\partial t^2} + 2\vec{\Omega} \times \frac{\partial \vec{r}}{\partial t} + \frac{\partial \vec{\Omega}}{\partial t} \times \vec{r} + \vec{\Omega} \times (\vec{\Omega} \times \vec{r}) \quad (8)$$

where $\frac{\partial^2 \vec{r}}{\partial t^2} = \vec{a}$ is the acceleration of an element relative to the translating and rotating frame of reference, and $\frac{\partial \vec{r}}{\partial t} = \vec{u}_*$ is the velocity of the element in this frame. The absolute acceleration of an element is thus

$$\vec{A} = \vec{U} + \vec{a} + 2\dot{\theta} \times \vec{u}_* + \ddot{\theta} \times \vec{r} + \dot{\theta} \times (\dot{\theta} \times \vec{r}) \quad (9)$$

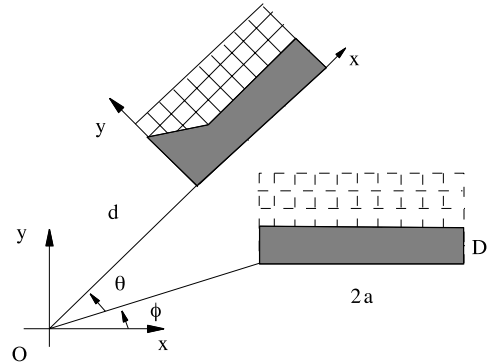


Figure 1. The Moving Coordinate System

This expression may be equated to the local force acting per unit mass of fluid to give the equation of motion in the moving frame. Here, \vec{U} is simply the apparent body force such as drift force, $2\dot{\theta} \times \vec{u}$ is the deflecting or Coriolis force, $\ddot{\theta} \times \vec{r}$ is referred to as the Euler force and $\dot{\theta} \times (\dot{\theta} \times \vec{r})$ is the centrifugal force. Thus, the body force term in the dynamic equation (6) is expressed in component form as

$$F_x = -g \sin \theta - \ddot{\theta} y + \dot{\theta}^2 x - d(\ddot{\theta} \sin \phi - \dot{\theta}^2 \cos \phi) - 2\dot{\theta} v \quad (10a)$$

$$F_y = g \cos \theta + \ddot{\theta} x + \dot{\theta}^2 y + d(\ddot{\theta} \cos \phi + \dot{\theta}^2 \sin \phi) + 2\dot{\theta} u \quad (10b)$$

where g is the gravitational acceleration and d is the distance between the origin of the moving coordinate and the axis of rotation.

Governing Equations

The equation governing the fluid motion (Eq. 5), including the pressure term in Equation (4) characterizing the limited compressibility and with the fluid mean density normalised to one, becomes

$$\frac{\partial u}{\partial t} + u \frac{\partial u}{\partial x} + v \frac{\partial u}{\partial y} + \frac{\partial p}{\partial x} = -g \sin \theta - 2\dot{\theta}v - \ddot{\theta}(y + d \sin \phi) + \dot{\theta}^2(x + d \cos \phi) + \nu \left(\frac{\partial^2 u}{\partial x^2} + \frac{\partial^2 u}{\partial y^2} \right), \quad (12a)$$

$$\frac{\partial v}{\partial t} + u \frac{\partial v}{\partial x} + v \frac{\partial v}{\partial y} + \frac{\partial p}{\partial y} = g \cos \theta + 2\dot{\theta}u + \ddot{\theta}(x + d \cos \phi) + \dot{\theta}^2(y + d \sin \phi) + \nu \left(\frac{\partial^2 v}{\partial x^2} + \frac{\partial^2 v}{\partial y^2} \right). \quad (12b)$$

Numerical stability and accuracy

In this section, the strengths and weaknesses of the numerical technique that affect the stability and accuracy, as well as the limitation on the extent of computation, will be discussed. In the numerical study, the flow field was discretized into many small control volumes. The equations of motion were then satisfied in each small control volume. Obvious requirements for accuracy include the necessity for the control volumes or cells to be small enough to resolve the features of interest, and for time steps to be small enough to prevent instability. Once a mesh has been chosen, the choice of the time increment necessary for stability is governed by two restrictions. First, fluid particles cannot move through more than one cell in one time step, because the difference equations assume fluxes only between adjacent cells. Therefore, the time increment must satisfy the inequality

$$\delta t < \min \left\{ \frac{\delta x_{i+1/2}}{|U_{i,j}|}, \frac{\delta y_{i+1/2}}{|V_{i,j}|} \right\} \quad (13)$$

where $\delta x_{i+1/2}$ and $\delta y_{i+1/2}$ are the half sizes of the cell in the x and y directions, respectively. Typically, δt is chosen equal to a time between one-fourth and one-third of the minimum cell transit time (Lou et al., 1980; Su et al., 1982). Second, when choosing a non-zero value of kinematic viscosity, momentum must not diffuse more than approximately one cell in one time step. A linear stability analysis (Lou et

$$\frac{1}{c^2} \frac{\partial p}{\partial t} + \frac{\partial u}{\partial x} + \frac{\partial v}{\partial y} = 0 \quad (11)$$

where all variables are now with respect to the tank-fixed coordinate system. Compressibility effects are included in the conservation mass equation (3) using equation(4), and in the momentum equation, fluid mean density is used. Thus the modified momentum equations yield the required expressions for two-dimensional flow in a rotating tank

al., 1980; Su et al., 1982) shows that this limitation implies

$$\nu \delta t < \frac{1}{2} \frac{\delta x_i^2 \delta y_j^2}{(\delta x_i^2 + \delta y_j^2)}. \quad (14)$$

The other parameter needed to insure numerical stability is α , which is the upstream differencing parameter. The parameter α is a weighting coefficient in an explicit scheme of the finite difference formulation of the momentum equation. If α is chosen to be 0, the advective terms in the momentum equation become centered differences. This situation is unstable in the absence of large physical viscosity as reported in Su et al. (1982). If α is chosen to be 1, the advective terms are evaluated using upstream differencing. Upstream differencing is diffusive and can yield an inordinate amount of numerical viscosity. Therefore, the combination of upstream and centered differencing may balance the diffusion-like truncation error and yield a stable algorithm. The proper choice for α is then (Lou et al., 1980; Su et al., 1982),

$$1 \geq \alpha \geq \max \left\{ \left| \frac{U_{i,j} \delta t}{\delta x_{i+1/2}} \right|, \left| \frac{V_{i,j} \delta t}{\delta y_{i+1/2}} \right| \right\}. \quad (15)$$

α is typically set to be 30-50% higher than the Courant number (c) where $c = \vec{V} \frac{\Delta t}{\Delta x} \leq 1$. In our computations, α is chosen to be 0.4 - 0.5. Formally, when considering the accuracy of a finite difference

scheme, the order of accuracy is defined by the lowest order powers of the increments of time and space appearing in the truncation error of the modified equation. A higher order scheme that is second order accurate, can be used to improve accuracy, but any process, that increases the accuracy of the results will also increase the computation time, and in most cases the relationship is non-linear. Another parameter that has an effect on the accuracy is ε . This is the criterion used to govern the level of mass conservation. For an incompressible fluid,

$$\nabla \cdot \vec{u} \leq \varepsilon \quad (16)$$

If ε is not zero, then the fluid is numerically compressible. Since it is extremely difficult to enforce zero divergence, a finite value must be used. Typical values are about $\varepsilon = 10^{-3}$. But it has been found that even larger values of epsilon do not seriously affect the results. Su et al. (1982) reported the similar results.

Numerical Implementations – Case Studies

Base of analysis

A total of 10 cases of computation were studied, as shown in the Table. It was assumed that the mesh dimensions would be small enough to resolve the main feature of liquid sloshing in each case. The step of time advance Δt , in each cycle was also assumed to be so small that no significant flow change would occur during Δt . There was no case where a steady state solution was reached during the forcing periods used. Either instability set in or computer time became excessive, so the duration of computation was limited for each case. Therefore, computations were halted when the fluid particles interact extremely and spray over the topside of the tank during extreme sloshing

When the frequency of the tank motion approaches one of the natural frequencies of the tank fluid, large sloshing amplitudes result. For a given tank geometry, the natural frequencies of the fluid depend on the fill depth and can be calculated from linear theories (Su et al., 1982). For rectangular prismatic tanks, the natural frequencies are given by

$$\omega_n^2 = g \frac{n\pi}{2a} \tanh\left(\frac{n\pi}{2a}D\right) \quad (17)$$

where, g is the gravitational acceleration, $2a$ is the tank width, D is the water depth and n is the mode number. As seen from the above equation, an infinite number of natural frequencies exist. However, only the fundamental frequency ($n=1$) is significant for marine engineering application (Su et al., 1982).

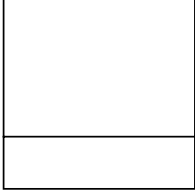
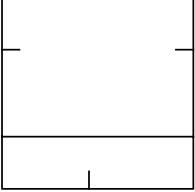
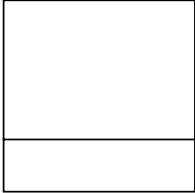
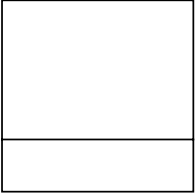
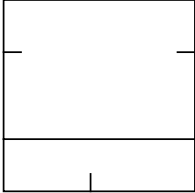
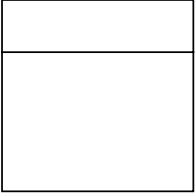
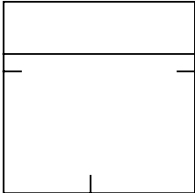
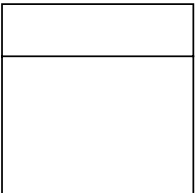
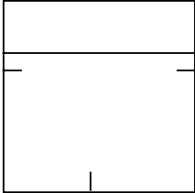
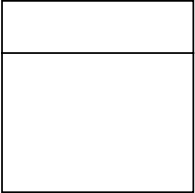
In all cases, the tank started to roll about the center of the tank bottom at time $t=0^+$. Since the major concern is to find the peak pressures on the left side of the tank on the free surface, the analysis is based on the comparison of the positive maximum pressures above the calm free surface for the various cases computed.

The effect of forcing frequency on shallow liquid sloshing

Cases (a), (c) and (d) in Table are the simulation in an unbaffled tank, with a roll amplitude of 8^0 and roll frequency ω_R equal to natural frequency ω_n , $0.75\omega_n$ and $0.65\omega_n$, respectively. The time for simulation is ended at 2.0 times the forcing period (T_f). Figures 2(i), 2(ii) and 2(iii) show that the maximum normalized pressures ($p/2\gamma a\theta_o$) in cases (a), (c) and (d) were obtained as 1.085 at $t^*=7.95$ [where $t^*=t(g/2a)^{0.5}$], 0.6975 at $t^*=9.14$, and 0.5979 at $t^*=11.07$, respectively. This indicates that the maximum pressure decreases as the forcing frequency becomes less than the linear resonant frequency of the fluid. The blanks in the figures indicate that the pressures on the left side of the tank take negative values below the calm free surface.

Cases (b) and (e) are from a baffled tank with a roll amplitude of 8^0 and roll frequency ω_R equal to ω_n and $0.75\omega_n$, respectively. The time for simulation is ended at 1.05 times the forcing period. During this period, as can be seen in Figures 2(iv) and 2(v), the maximum pressure in case (b) was 0.3959 at $t^*=4.38$ and in case (d) was 0.3467 at $t^*=5.13$ respectively. This indicates that the maximum pressure in baffled tanks decrease as the forcing frequency becomes less than the linear resonant frequency of the fluid. The simulation time for both baffled cases is relatively short compared with the unbaffled cases because of the severe effects of wave breaking and spraying. Therefore, only first peak pressures were obtained in the baffled cases as opposed to multiple consecutive peaks obtained with the unbaffled cases.

Table Cases of Computations (Mesh Dimensions = 41 x 30, H = Height of the Tank)

<p>Case (a)</p> 	<p>Tank Dim.=60*60 feet Fill Depth=0.25*H Natural Frequency: $\omega_n = 1.0511 \text{ rad / sec}$ Roll Amplitude = 8° Roll Freq.: $\omega_R = \omega_n$</p>	<p>Case (b)</p> 	<p>Tank Dim.=2*2 feet Fill Depth=0.25*H Natural Frequency: $\omega_n = 5.757 \text{ rad / sec}$ Roll Amplitude=8° Roll Freq.: $\omega_R = \omega_n$</p>
<p>Case (c)</p> 	<p>Tank Dim.=60*60 feet Fill Depth=0.25*H Natural Frequency: $\omega_n = 1.0511 \text{ rad / sec}$ Roll Amplitude=8° Roll Freq.= $\omega_R = 0.75\omega_n$</p>	<p>Case (d)</p> 	<p>Tank Dim.=60*60 feet Fill Depth=0.25*H Natural Frequency: $\omega_n = 1.0511 \text{ rad / sec}$ Roll Amplitude=8° Roll Freq.= $\omega_R = 0.85\omega_n$ $\omega_R = 0.65\omega_n \text{ (sec 4.2)}$</p>
<p>Case (e)</p> 	<p>Tank Dim.=2*2 feet Fill Depth=0.25*H Natural Frequency: $\omega_n = 5.757 \text{ rad / sec}$ Roll Amplitude=8° Roll Freq.= $\omega_R = 0.85\omega_n$ $\omega_R = 0.75\omega_n$</p>	<p>Case (f)</p> 	<p>Tank Dim.=60*60 feet Fill Depth=0.75*H Natural Frequency: $\omega_n = 1.2863 \text{ rad / sec}$ Roll Amplitude=4° Roll Freq.: $\omega_R = \omega_n$</p>
<p>Case (g)</p> 	<p>Tank Dim.=2*2 feet Fill Depth=0.75*H Natural Frequency: $\omega_n = 7.0455 \text{ rad / sec}$ Roll Amplitude=8° Roll Freq.: $\omega_R = \omega_n$</p>	<p>Case (h)</p> 	<p>Tank Dim.=60*60 feet Fill Depth=0.75*H Natural Frequency: $\omega_n = 1.2863 \text{ rad / sec}$ Roll Amp.= 4° and 8° Roll Freq.= $\omega_R = 0.85\omega_n$</p>
<p>Case (i)</p> 	<p>Tank Dim.=2*2 feet Fill Depth=0.75*H Natural Frequency: $\omega_n = 7.0455 \text{ rad / sec}$ Roll Amplitude=8° Roll Freq.= $\omega_R = 0.85\omega_n$</p>	<p>Case (j)</p> 	<p>Tank Dim.=60*60 feet Fill Depth=0.75*H Natural Frequency: $\omega_n = 1.2863 \text{ rad / sec}$ Roll Amp.= 4° and 8° Roll Freq.: $\omega_R = \omega_n$</p>

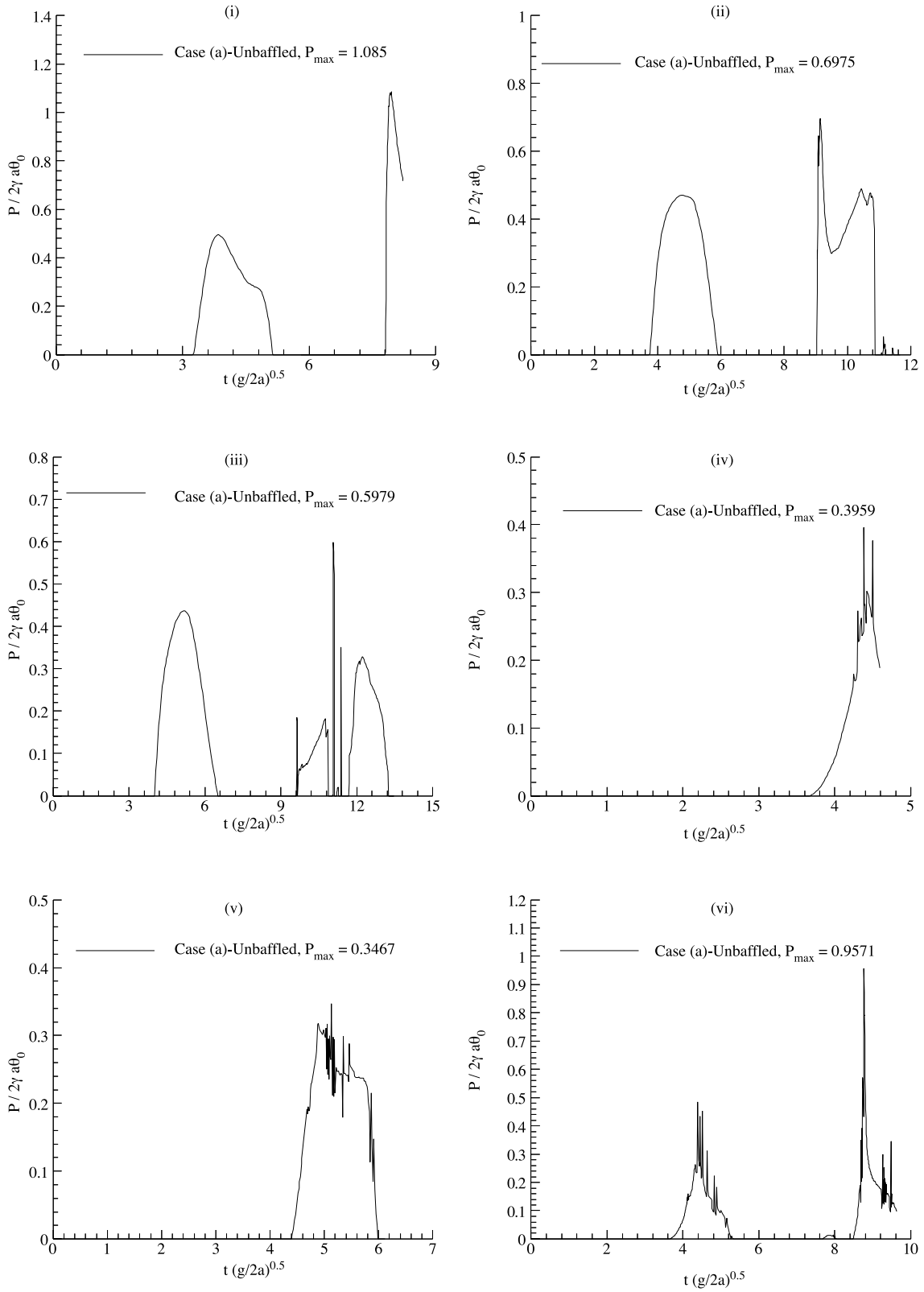


Figure 2. The Maximum Pressures in Shallow Liquid Sloshing

The effect of baffling on shallow liquid sloshing

Case (a) in Table , on a resonant frequency with a roll amplitude of 8^0 , represents shallow liquid sloshing in an unbaffled tank. Another run is made with the baffles to obtain the shallow water effects. The simulation length is taken as 2.2 times the forcing period. Figures 2(i) and 2(vi) show that the maximum pressure in case (a) without a baffle was 1.085 at $t^* = 7.95$ and with a baffle it was 0.9571 at $t^* = 8.77$. It can be concluded that the baffle located vertically on the center of the bottom tended to reduce the maximum pressure on the sides of the tank.

Case (d), on an off resonant frequency ($0.85\omega_n$) with a roll amplitude of 8^0 , represents shallow liquid sloshing in an unbaffled tank. Another run is made with the baffles. For both cases the simulation times are ended at 1.143 times the forcing period. Figures 3(i) and 3(ii) show that baffles cause a significant pressure fluctuation and overall pressure decrease compared to the unbaffled case. The major source of fluctuation is due to the vertices at the both sides of the vertical baffle located at the centre of the tank bottom. Furthermore, the flow over a vertical baffle produces a shear layer and energy is dissipated by the viscous action. This may cause the reduction in pressure.

The effect of fill depth in an unbaffled tank

Cases (a) and (j), on a resonant frequency with a roll amplitude of 8^0 , represent the liquid sloshing with different fill depths. In both cases, simulations are halted at 1.34 times the forcing period. Figures 3(iii) and 3(iv) indicate that the maximum pressure in case (j) is almost 2 times greater than that of the shallow water case (a). In case (j), the maximum pressure results from the water impact on the tank top. The pressure fluctuations near the peak in Figure 3(iv) are basically due to the interactions between the wave and tank top.

Cases (d) and (h) represent the liquid sloshing with different fill depths for an off resonant frequency of ($0.85\omega_n$) with a roll amplitude of 8^0 . The numerical results up to $t = 2.0T_f$ were analyzed. Due to off resonant sloshing, the interaction between the wave and the tank top is relatively less severe compared to cases (a) and (j). This results in a more stable computation and thus a greater simulation time. The severe fluctuations in Figure 3(vi) are caused by continuously repeated interactions between the wave and the tank top.

The effect of fill depth in a baffled tank

Cases (b) and (g), on a resonant frequency with a roll amplitude of 8^0 , represent liquid sloshing with different fill depths in a baffled tank. As can be seen in Figures 4(i) and 4(ii), the simulation time is halted at 1.05 times the forcing period. The amount of maximum pressure in Figure 4(ii) is approximately five times greater than that of the shallow water case in Figure 4(i). The possible cause for this high pressure may be due to the non linear softening effect of baffling and shallow water due to the horizontal baffles. The shallow water effect dissipates energy by forming a hydraulic jump and a breaking wave.

Cases (e) and (i), on an off resonant frequency of ($0.85\omega_n$) with a roll amplitude of 8^0 , represent the liquid sloshing with different fill depths. The magnitude of pressure in shallow water cases, shown in Figures 4(i) and 4(iii), is decreased approximately by 5% while the magnitude of pressure in deep water cases in Figures 4(ii) and 4(iv) is decreased approximately by 16%. The large pressure fluctuations in Figures 4(iii) and 4(iv) may result from possible severe non linear effects around the vertical and horizontal baffles. The location of maximum pressures is shifted forward approximately by 6% of t^* compared to the resonant cases in Figures 4(i) and 4(ii).

The effect of forcing frequency on deep water sloshing

Cases (j) and (h) in an unbaffled tank with a roll amplitude of 8^0 are studied for roll frequencies ω_R equal to ω_n and $0.85\omega_n$, respectively. During the simulation, the maximum pressure was 0.9201 in case (h) at $t^* = 3.66$ and was 0.9697 in case (j) at $t^* = 3.37$ [See Figures 4(v) and 4(vi)]. It is seen that the pressure fluctuations in Figure 4(vi) are more than those in Figure 4(v). The location of maximum pressure in a resonant condition is shifted back (9% of t^*) compared to the off resonant condition. The results also show that the maximum pressure decreases as the forcing frequency becomes less than the linear resonant frequency of the fluid.

Cases (g) and (i), in a baffled tank, are with a roll amplitude of 8^0 and roll frequencies ω_R equal to ω_n and $0.85\omega_n$, respectively. Figures 5(i) and 5(ii) show that the maximum pressure in an off resonant case is reduced approximately by 16% compared to the resonant case and the location of maximum pressure is 6% shifted forward in case of off resonant conditions.

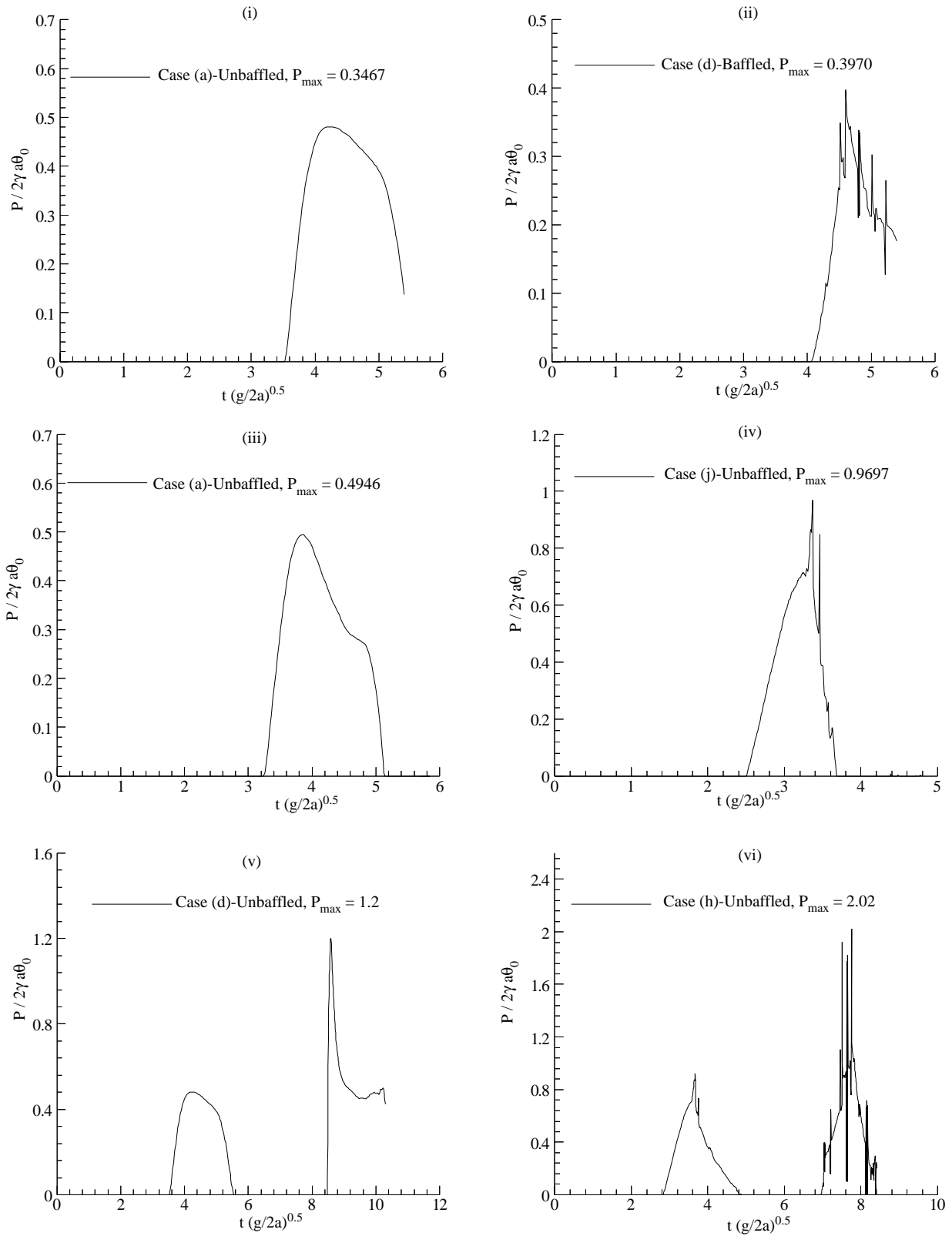


Figure 3. The Maximum Pressures in Different Baffle Configurations and Fill Depth

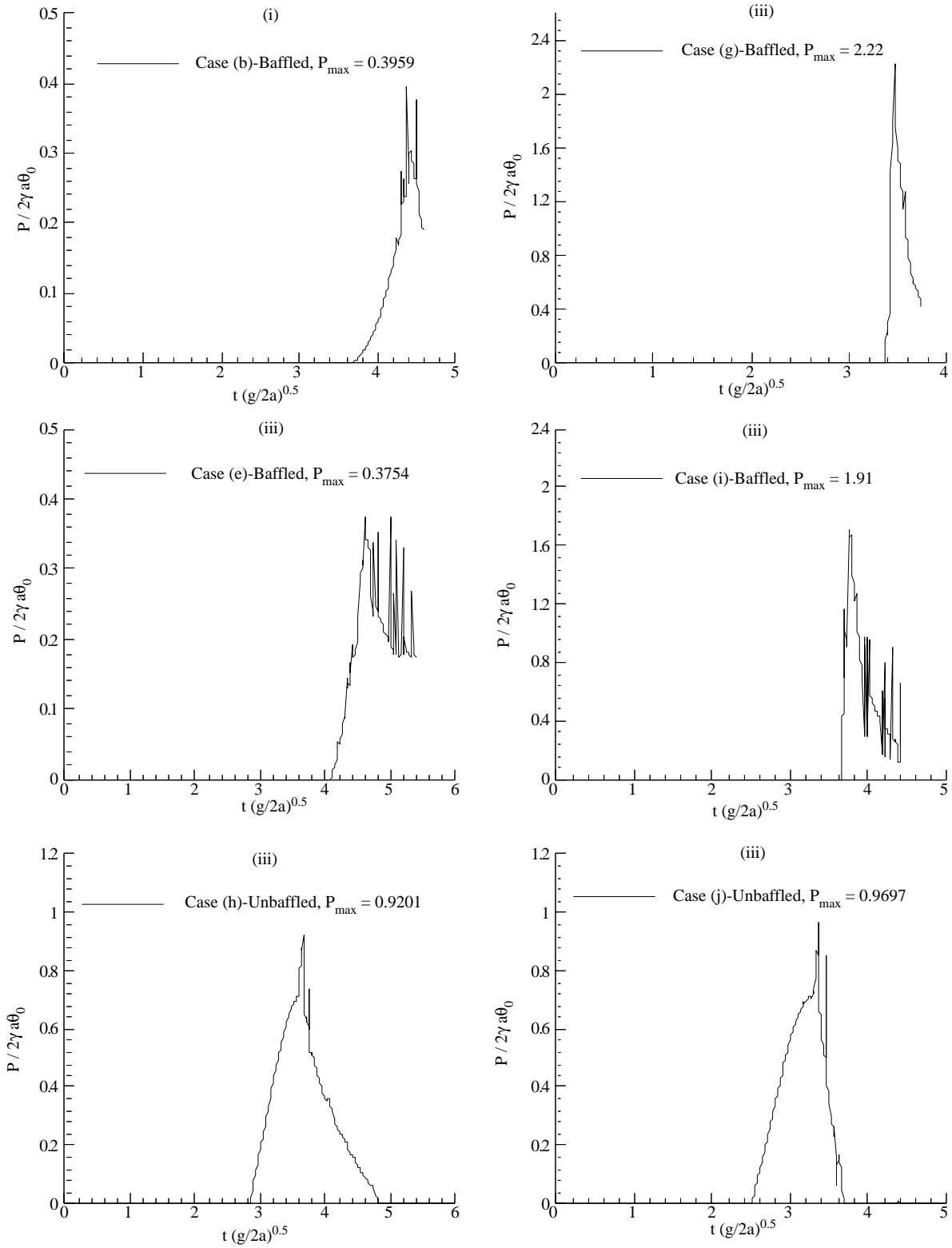


Figure 4. The Maximum Pressures in Different Baffle Configurations and Forcing Frequency

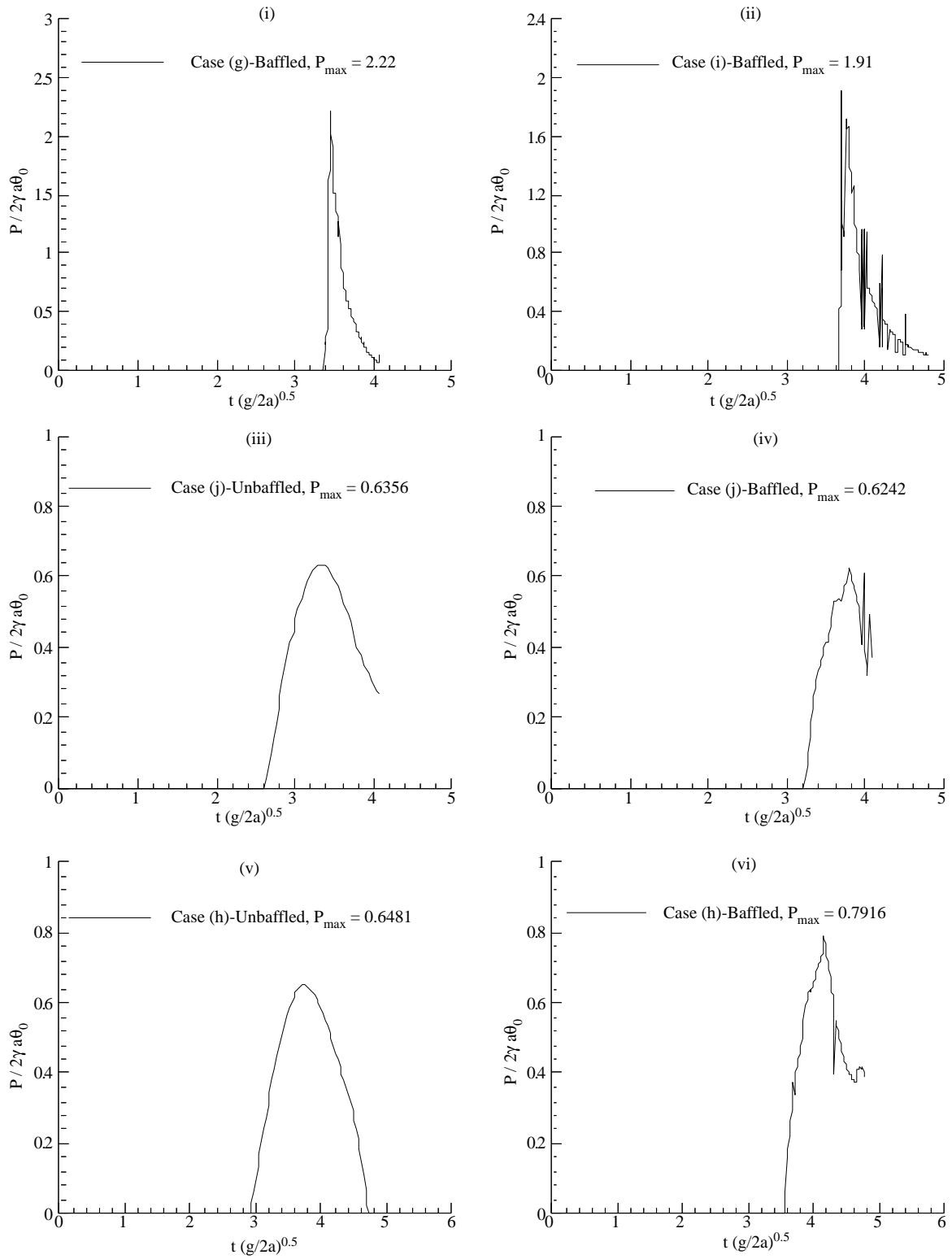


Figure 5. The Maximum Pressures in Deep Water Liquid Sloshing

The effect of baffle in deep water sloshing

Case (j), on resonant frequency with a roll amplitude of 4° , represents deep water sloshing in an un-baffled tank. Another run, for comparison, is made with baffles. It can be concluded from Figures 5(iii) and 5(iv) that baffles slightly decreased the maximum pressure (1.8%). For baffled cases, a horizontal baffle was installed to force the hydraulic jump to stay or wave breaking to occur on top of the horizontal baffle so that the impact load associated with breaking waves would not act on the tank wall. From the numerical experiments, it appears that this horizontal baffle enhances the travelling characteristics of the sloshing wave, which may result in a slamming pressure. Horizontal baffles also enhance the adverse pressure gradients resulting from wall boundary conditions. Therefore, pressure fluctuations, shown in the Figure 5(iv), may result from these non linear effects of the horizontal baffles.

Case (h), which includes off resonant frequency with a roll amplitude of 4° , represents deep water sloshing in unbaffled and baffled tanks. The maximum pressure in a baffled case in Figure 5(vi) is increased approximately by 20% than that of the unbaffled case in Figure 5(v). We can conclude from Figures 5(v) and 5(vi) that the baffle increases the

pressure slightly instead of reducing the maximum pressure because of the shallow water character induced by this baffle configuration.

The Effect of amplitude of excitation on sloshing in deep fill depth

Cases (f) and (j), on resonant frequency with roll amplitudes of 4° and 8° , represent liquid sloshing in an unbaffled tank. Figures 6(i) and 6(ii) show that the maximum pressure in 8° roll amplitude, increased approximately by 54% compared to the 4° roll amplitude, while the location of the peak pressure remains almost constant at $t^* = 3.35$. Furthermore, the pressure fluctuations in 8° roll amplitude are more severe than that of 4° roll amplitude, because in these cases, a large amplitude standing wave has built up as the rolling amplitude increases. The pressure distribution on the tank wall is mainly due to the hydrostatic effect.

As an example for all cases, in Figure 7, a snapshot at $t^* = 3.3$ for both baffled and unbaffled conditions is presented for case (j). Results show that with the baffles on the sides, the sloshing was damped relatively while pressure decreased and fluctuation increased.

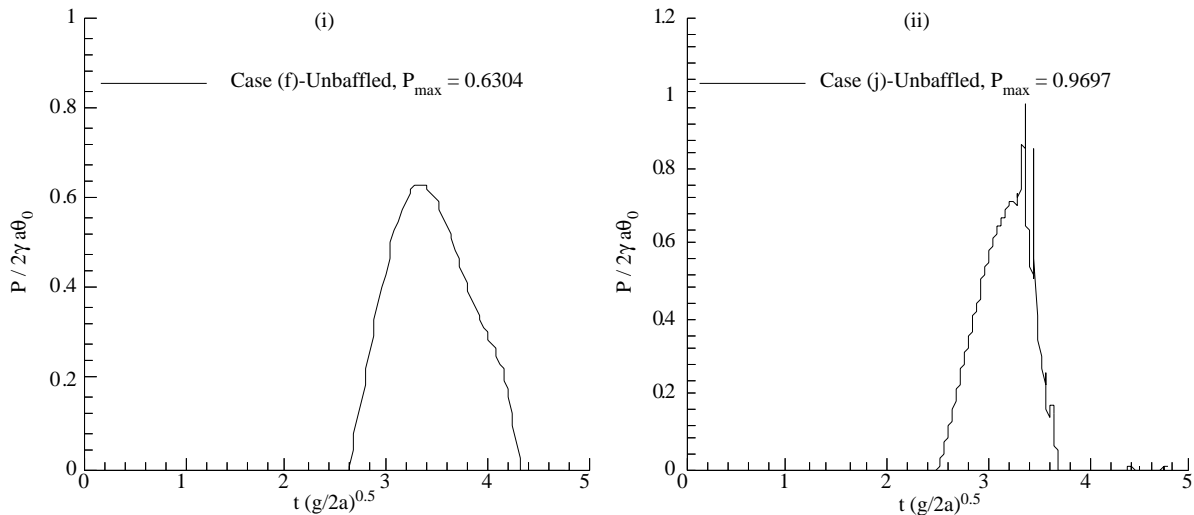


Figure 6. The Maximum Pressures in Different Amplitudes of Excitation

Comparisons with Theoretical and Experimental Results

In order to assess the accuracy of the method used, computations are compared with the theoretical and experimental results given in the final re-

port by Lou et al., (1980). The comparisons of the dimensionless maximum pressures computed numerically versus dimensionless excitation frequencies (or rolling periods) are presented in terms of time simulation in Figures 8 and 9. In Figure 8, a fill depth of 0.15 H (tank height = 3ft) and a roll amplitude

of 1° are taken as a tank configuration. Fill depth of 0.40 H (tank height = 2ft) and a roll amplitude of 8° are taken as another tank configuration in Figure 9. Numerical results show that as the simulation time increased, the maximum pressures, especially near the resonance frequency, also increased. The upper

limit for simulation time is taken as the commencement of severe splashing at the tank top, which is $t = 4.0 * T_f$ for $\theta = 1^\circ$ and $t = 3.0 * T_f$ for $\theta = 8^\circ$, respectively. The same figures also show that the maximum pressures at the off resonance frequencies are not significantly changed in both cases.

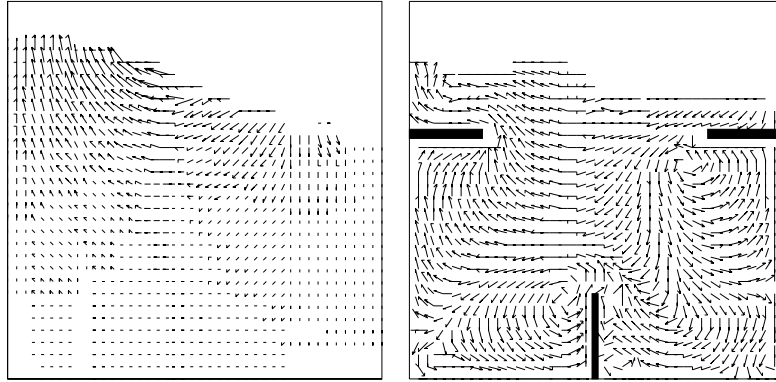


Figure 7. Snapshot in Case (j) with an Unbaffled and Baffled Condition at $t^* = t / (g / 2a)^{0.5} = 3.3$

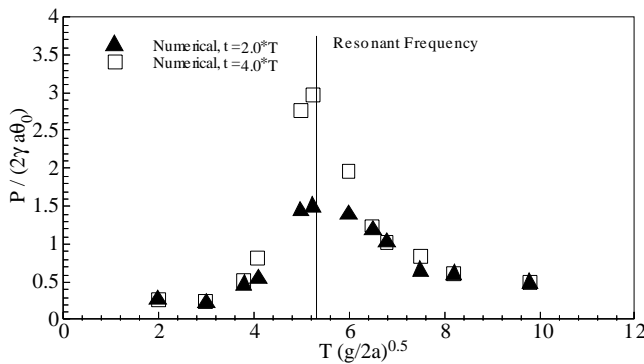


Figure 8. Comparison of Numerical Solutions at Different Simulation Time; $\theta = 1^\circ$, Tank Length = 3 ft.

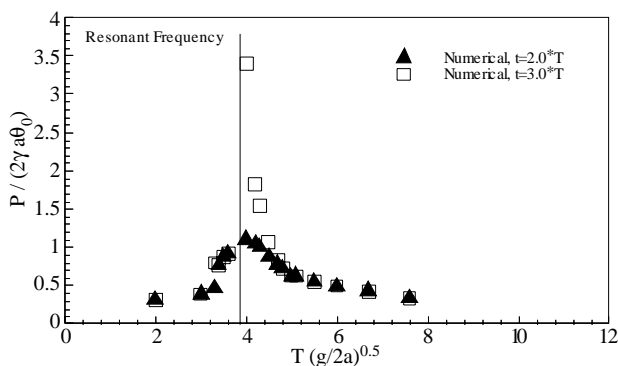


Figure 9. Comparison of Numerical Solutions at Different Simulation Time; $\theta = 8^\circ$, Tank Length = 2 ft.

The comparisons of the analytical solutions and experimental results with our numerical results are shown in Figures 10 and 11. The analytical solution and experimental result agreed very well with the numerical solution at a simulation time of $t = 4 * T_f$. Figure 10 shows that the agreement between numerical and experimental results is better, especially near the resonance frequency and lower frequencies. Furthermore, it can be concluded that for smaller fill depths and roll amplitudes, the agreement is better. In Figure 11, the maximum pressures computed numerically at a simulation time of $t = 3 * T_f$ are not in good agreement compared to the previous case due to the increased fill depth and rolling amplitude. In the resonance region, numerical results agreed very well with the analytical and experimental results, on the other hand, the agreement in the off resonance regions is not as good as in the previous case.

Conclusions

The volume of fluid technique has been used to simulate two-dimensional viscous liquid sloshing in moving rectangular baffled and unbaffled tanks. The VOF method was also used to track the actual positions of the fluid particles on the complicated free surface. The liquid was assumed to be homogeneous and flow was assumed to remain laminar. The exci-

tation was assumed to be harmonic after the motion starts from rest. A moving coordinate system fixed in the tank was used to simplify the boundary condition on the fluid tank interface during large tank motions.

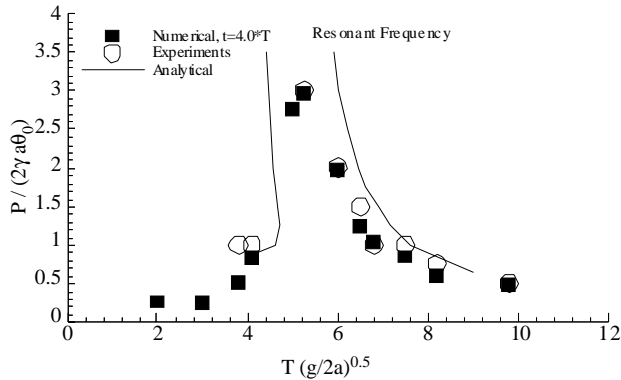


Figure 10. Comparison of Numerical Solutions with Experimental Results and Analytical Solutions; $\theta = 1^\circ$, Tank Length = 3 ft.

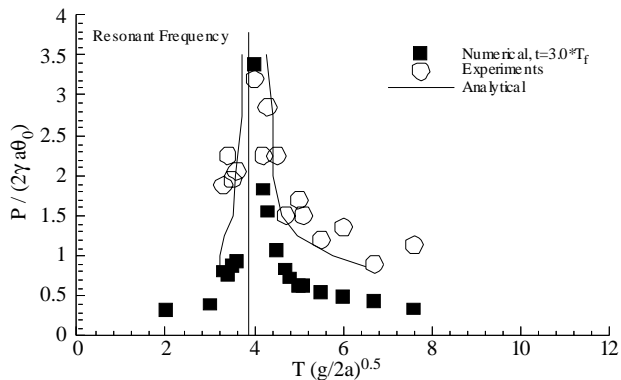


Figure 11. Comparison of Numerical Solutions with Experimental Results and Analytical Solutions; $\theta = 8^\circ$, Tank Length = 2 ft.

The general features of the effects of various baffles on liquid sloshing inside the partially filled enclosed tanks were studied. The following results can be drawn from our numerical computations:

- i) When the amplitude of excitation was large, the liquid responded violently, which caused the numerical solution to become unstable. The applicability of the method used in the present study is limited to the period prior to the inception of the instability.
- ii) Various baffles on liquid sloshing inside a tank revealed that the flow over a vertical baffle produced a shear layer and energy was dissipated

by the viscous action. Flow over a horizontal baffle exhibited a shallow water character, which dissipated energy by forming a hydraulic jump and a breaking wave.

iii) The effect of vertical baffles was most pronounced in shallow water. On the other hand, the horizontal baffle was more effective in introducing the shallow water effects in the deep water case. Furthermore, it is indicated that the horizontal baffle may enhance the traveling characteristic of the sloshing wave, which could result in a higher slamming pressure.

iv) It can be concluded from the limited number of numerical tests that the combination of a pair of horizontal baffles, one at each end of the tank and a short vertical baffle at the bottom center seemed to be a practical arrangement that could be effective over a range of fill depths. But this conclusion needs to be supported by both experimental results and extensive numerical tests.

v) The increased fill depth and roll amplitude of the tank directly effects the degree of non linearity of the sloshing phenomena. The possible sources for non linearity are the occurrence of turbulence around the baffles, the spraying of fluid particles due to interaction with the tank top and wave breaking on the free surface.

Finally, the effects of turbulence and two-phase flow (sprays, drops and bubbles in the post impact period) as well as three-dimensional effects need to be incorporated to assure a stable and reliable modeling for such cases. For future work, second-order representation of derivatives may be employed to better approximate to the rapid change of divergence in the fluid. The effect of speed of sound, in the case of extreme sloshing, has to be checked to see the compressibility effect to some degree.

Nomenclature

\vec{V}_n : The normal component of the fluid velocity
 \vec{V}_t : The tangential component of the fluid velocity
 P : Fluid pressure
 P_{ATM} : Atmospheric pressure
 ν : Kinematic viscosity
 ρ : Fluid density
 n_x, t_x : The corresponding horizontal values of the components of the unit vector
 n_y, t_y : The corresponding vertical values of the components of the unit vector
 \vec{F} : Body forces
 θ : Roll angle
 ϕ : The equilibrium angle of the tank relative to the axis of rotation

d : The distance between the origin of the moving coordinate and the axis of rotation
 D : Fill depth
 $2a$: Tank length
 $\vec{\Omega}$: Angular velocity
 \vec{U} : Acceleration of the moving frame
 \vec{a}^* : Acceleration of an element relative to the point O
 δt : Time increment
 α : The upstream differencing parameter
 ε : The compressibility parameter
 ω_R : Roll frequency
 ω_n : Natural frequency
 T_f : Forcing period
 H : Height of the tank

Acknowledgment

The authors would like to thank to Research Fund of Istanbul Technical University for the financial support of this study.

References

Abramson H.N., "Dynamic Behavior of Liquids in Moving Containers with Application to Space Vehicle Technology", NASA-SP-106, 1966.

Celebi M.S., Kim M.H. and Beck R.F., "Fully Non-linear 3-D Numerical Wave Tank Simulation", J. of Ship Research, 42(1), 33-45, 1998.

Dillingham J., "Motion Studies of a Vessel with Water on Deck", Marine Technology, SNAME, 18(1), 38-50, 1981.

Faltinsen O.M., "A Nonlinear Theory of Sloshing in Rectangular Tanks", J. of Ship Research, 18(4), 224-241, 1974.

Faltinsen O.M., "A Numerical Nonlinear Method of Sloshing in Tanks With Two-Dimensional Flow", J. of Ship Research, 22(3), 193-202, 1978.

Feng G.C., "Dynamic Loads Due to Moving Liquid", AIAA Paper 73-409, 1973.

Harlow F.H. and Welch J.E., "Numerical Calculation of Time Dependent Viscous Incompressible Flow", Phys. Fluids 8, 2182, 1965.

Hirt C.W. and Nichols B.D., "Volume of Fluid Method for the Dynamics of Free Boundaries", Journal of Computational Physics, 39, 201-225, 1981.

Lee D.Y. and Choi H.S., "Study on Sloshing in Cargo Tanks Including Hydro elastic Effects", J. of Mar. Sci. Technology, 4(1), 1999.

Lou Y.K., Su T.C. and Flipse J.E. "A Nonlinear Analysis of Liquid Sloshing in Rigid Containers", US Department of Commerce, Final Report, MA-79-SAC-B0018, 1980.

Lui A.P. and Lou J.Y.K., "Dynamic Coupling of a Liquid Tank System Under Transient Excitations", Ocean Engineering, 17(3), 263-277, 1990.

Nakayama T. and Washizu K., "Nonlinear Analysis of Liquid Motion in a Container Subjected to Forced Pitching Oscillation", Int. J. for Num. Meth. in Eng., 15, 1207-1220, 1980.

Roache P.J., "Computational Fluid Dynamics", Hermosa Publishers, Albuquerque, New Mexico, 1972.

Solaas F. and Faltinsen O.M., "Combined Numerical and Analytical Solution for Sloshing in Two-Dimensional Tanks of General Shape", Journal of Ship Research, 41(2), 118-129, 1997.

Su T.C., Lou Y.K., Flipse J.E. and Bridges T.J., "A Numerical Analysis of Large Amplitude Liquid Sloshing in Baffled Containers", US Department of Transportation, Final Report, MA-RD-940-82046, 1982.

Von Kerczek C.H., "Numerical Solution of Naval Free-Surface Hydrodynamics Problems", 1st International Conference on Numerical Ship Hydrodynamics, Gaithersburg, USA, 1975.